文章编号：1001-9014(XXXX)XX-0001-05

DOI:10.11972/j.issn.1001-9014.XXXX.XX.001

Extracting the effective mass of fewer layers 2D h-BN nanosheets using the Fowler Nordheim tunneling model

Qin Jia-Yi[1], Luo Man[1,2*], Cheng Tian-Tian[1], Meng Yu-Xin[1], Zu Yuan-Ze[1], Wang Xin[1], Yu Chen-Hui[1*]

(1. Jiangsu Key Laboratory of ASIC Design, School of Information Science and Technology, Nantong University, Nantong 226019, China;
2. State Key Laboratory of Infrared Physics, Shanghai Institute of Technical Physics, Chinese Academy of Sciences, Shanghai 200083, China)

Abstract: Hexagonal boron nitride (h-BN) finds widespread application, including gate dielectrics, passivation layers, and tunneling layers, owing to its outstanding properties. The current studies on the fundamental physical properties of these ultrathin h-BN films and the electron tunneling effect among them are inadequate. In this work, the effective mass in h-BN was successfully determined through a combined approach of experimental and theoretical research methods by fitting the current-voltage curves of metal/insulator/metal structures. It was observed that within a range of 4~22 layers, the effective mass of h-BN exhibits a monotonic decrease with an increase in the number of layers. Precisely ascertain the physical parameters of the Fowler-Nordheim tunneling model in the context of electron tunneling in h-BN by utilizing the extracted effective mass. Additionally, the impact of fixed charges at the metal/h-BN interface and various metal electrode types on Fowler-Nordheim tunneling within this structure was investigated utilizing this physical parameter in Sentaurus TCAD software. This work is informative and instructive in promoting applications in the fields of h-BN related infrared physics and technology.

Key words: h-BN, 2D layered material, Fowler-Nordheim tunneling, gate dielectrics, TCAD simulation
PACS:

基于Fowler-Nordheim隧穿模型提取层状h-BN的有效质量参数

秦嘉怡[1], 罗 曼[1,2*], 成田恬[1], 孟雨欣[1], 祖源泽[1], 王 鑫[1], 余晨辉[1*]

(1. 南通大学 信息科学技术学院 江苏省专用集成电路设计重点实验室,江苏 南通 226019;
2. 中国科学院上海技术物理研究所 红外物理国家重点实验室,上海 200083)

摘要:六方氮化硼(h-BN)由于其优良特性被广泛应用于栅介质层、钝化层、隧穿层等功能。目前,对关于超薄h-BN的基本物理性质和其中的电子隧穿效应的研究还存在不足。本文采用实验与理论相结合的研究方法,通过拟合金属/绝缘体/金属结构的电流-电压曲线成功提取了不同层数h-BN的有效质量。结果显示在4~22层范围内,h-BN的有效质量随着层数的增加而单调下降。文中利用已提取的有效质量精确确定当h-BN中发生电子隧穿时,Fowler-Nordheim隧穿模型的物理参数。此外,本文使用该物理参数在Sentaurus TCAD软件中研究了金属/h-BN界面处固定电荷以及不同种类的金属电极对该结构中Fowler-Nordheim隧穿的影响。这项工作对促进h-BN相关红外物理和技术领域的应用具有一定的参考和指导意义。

关 键 词:六方氮化硼;二维层状材料;Fowler-Nordheim隧穿;栅极电介质;TCAD仿真

INTRODUCTION

Hexagonal boron nitride (h-BN) features a layered honeycomb structure comprising boron and nitrogen rings, as shown in Fig. 1a[1-6]. The unique crystal structure grants h-BN an impressive array of properties, including wide bandgap, low dielectric constant, high breakdown voltage, exceptional chemical stability, flat surface free from dangling bonds and charged impurities[7-13]. These remarkable attributes firmly establish h-BN as an exemplary dielectric material, garnering widespread utilization in pioneering micro- and nano- electronic device applications. Furthermore, it's worth noting that h-BN displays opposite signs for its in-plane and out-of-plane relative dielectric constants within the mid-

Foundation items: Supported by the National Natural Science Foundation of China (62074085 and 62104118)
Biography: QIN Jia-Yi (1999-), female, master. Research area involves the design optimization of semiconductor devices. E-mail: qjyntu@126.com
* **Corresponding author**: E-mail: luoman@ntu.edu.cn; ychyu@ntu.edu.cn

infrared band[14]. This unique behavior suggests that h-BN can be excited to produce particularly strong phonon resonances in the mid-infrared band. Due to this characteristic, it has been used to design high-performance electro-optic devices, such as electro-optic modulators, absorbers, and detectors[15-18]. Its potential in optical applications, particularly in the realm of infrared optoelectronics, remains highly promising.

Fig. 1b illustrates the energy band diagram of a typical metal/insulator/metal (MIM) structure. When a positive voltage ($V<\varphi_0$) is applied to metal2 (M2), the Fermi level (E_F) of M2 decreases (Fig. 1c), leading to the flow of electrons across the whole trapezoidal barrier, which corresponds to the direct tunneling (DT). Conversely, upon increasing the applied bias voltage ($V>\varphi_0$), the Fowler-Nordheim (FN) tunneling becomes prominent, where electrons tunnel through a triangular potential barrier, as illustrated in Fig. 1d. While h-BN layers with different thicknesses have been extensively utilized in device fabrication, previous research efforts have primarily focused on investigating the overall electrical properties of these devices[19-25]. However, the intrinsic physical properties of h-BN layers with different thicknesses have received limited attention.

In this paper, with the combination of experimental and theoretical research methods, we have successfully extracted the effective mass in ultrathin h-BN layers through simulating the current-voltage (I-V) curves of MIM structures. It is found that the effective mass in h-BN exhibits a consistent decrease as the number of atomic layers increases within the nanometer range. This phenomenon underscores the high susceptibility of the physical properties of a few h-BN layers to external factors. Moreover, through effective mass calculations linked to the number of layers, we can precisely determine the physical parameters of the FN tunneling model during electron tunneling in h-BN. This has significant implications for optimizing the design and utilization of gate dielectric and tunneling layers. This work provides valuable insights and hold crucial relevance for promoting applications in the domain of h-BN-based infrared physics and technology.

1 Calculation method

It has been verified that the tunneling process in h-BN is predominantly governed by the FN tunneling process under high bias voltages. The corresponding tunneling current is nonlinearly expressed as[19-22]:

$$I(V) = S_{eff} \times A \times F_{ins}^2 \times \exp\left(\frac{-B}{F_{ins}}\right) \tag{1}$$

where $A = \frac{q^3 m}{8\pi h \varphi_B m^*}$; $B = \frac{8\pi\sqrt{2m^*}\,\varphi_B^{\frac{3}{2}}}{3hq}$; and the electric field in the insulator $F_{ins} = \frac{V}{d}$. Thus, formula (1) can be re-expressed in the following form:

$$\ln\frac{I(V)}{V^2} = \ln\frac{S_{eff} q^3 m}{8\pi h \varphi_B d^2 m^*} - \frac{8\pi\sqrt{2m^*}\,\varphi_B^{\frac{3}{2}} d}{3hqV} \tag{2}$$

where S_{eff} and φ_B are effective tunneling area and barrier height, respectively; h is Planck's constant; d is the thickness of the insulator h-BN; V is the applied bias voltage; and m^* is the effective mass of the electrons in the conduction band of h-BN.

Prior research has explored the tunneling process of electrons in ultra-thin h-BN with thickness exceeding 4 layers[22]. However, the impact of layer variation of 2D materials with a limited number of layers on intrinsic physical properties has been underappreciated in the past, such as bandgap and effective mass[26]. In this work, we adopt an improved research method for FN tunneling. By emulating the experimental the electric properties of MIM structures, we extract the effective mass and S_{eff} concerning different h-BN layer numbers. In line with conventional methods for processing physical data, we attribute all other non-ideal factors with layer dependency to effective mass. The detailed calculation method and process are outlined below. In order to obtain $ln(I/V^2)$-$1/V$ curve, a mathematical transformation is applied to the experimental I-V curve of a h-BN film, as shown in the inset of Fig. 2a. Subsequently, the curve is subjected to fitting analysis to determine the slope value, which can be known according to formula (2):

$$slope = -\frac{8\pi\sqrt{2m^*}\,\varphi_B^{\frac{3}{2}} d}{3hq} \tag{3}$$

Give that the h-BN affinity energy is 2 eV[27-29] and the work function of Gold is 5 eV[30-31], the barrier height φ_B can be determined. By substituting this value into formula (3), the effective mass of electrons in h-BN can be calculated out. Thereafter, the two essential physical parameters, A and B, within the FN tunneling formula can be derived.

To determine the S_{eff} of h-BN at different layers, current-voltage values are extracted from the I-V curve in

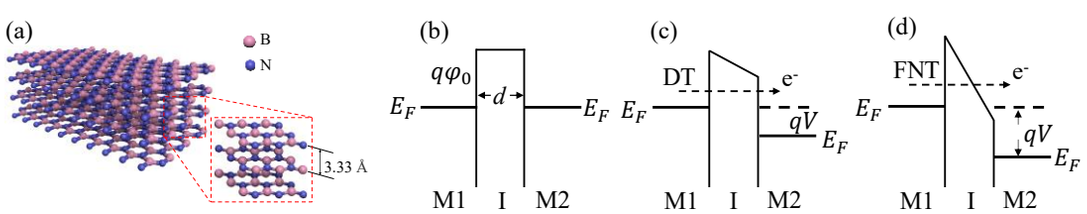

Fig. 1 (a) Crystal structure of h-BN. Red dash lines represent the unit cell[2]. Energy bands of the MIM structure: (b) V=0; (c) $V<\varphi_0$; (d) $V>\varphi_0$

图1 (a) h-BN的晶格结构。红色虚线框中表示单位晶胞[2]。MIM结构的能带示意图(b) V=0;(c) V<φ0;(d) V>φ0

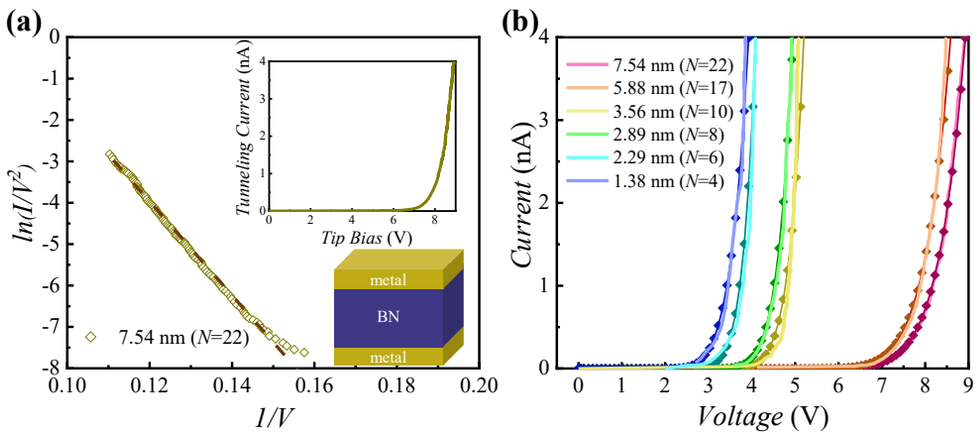

Fig. 2 (a) $ln(I/V^2)$-1/V curve and its fitting curve for $d_{h\text{-}BN}$=7.54 nm. The inset shows the experimental I-V curve of one MIM structure. (b) Comparison of theoretical and experimental values of FN tunneling with N representing the number of layers
图2 (a) dh-BN=7.54 nm时ln(I/V2)-1/V曲线及其拟合曲线。插图显示了MIM结构及I-V曲线实验值。(b) FN隧穿电流理论值与实验值对比,其中N表示层数。

Fig. 2a. These values are then used in tunneling current formula (1). Subsequently, the comprehensive average of the tunneling area is obtained. The S_{eff} calculated reaches a satisfactory agreement with the device size of 25 nm (±10 nm) reported in this experiment. As a consequence, the validity of the h-BN effective mass value calculation is further affirmed from this juncture. Table 1 summarizes the calculated physical quantities for h-BN layers with varying layers from Ref. 22, including the effective mass, the S_{eff}, the parameters A and B of the FN tunneling model. For $d_{h\text{-}BN}$=1.38 nm, the calculated S_{eff} is three orders of magnitude smaller than for other thicknesses. This discrepancy may be attributed to the extreme thinness of the h-BN, which can lead to uneven film thickness or irregular gap distances between the h-BN layer and the metal material during the experimental process[32].

Table 1 Calculated physical quantities corresponding to different h-BN thicknesses
表1 计算得到的不同h-BN厚度时对应的物理量

$d_{h\text{-}BN}$	layers	m^*/m	S_{eff} (cm^2)	A (A/V^2)	B (V/cm)
7.54 nm	22	0.184216	4.116×10^{-12}	2.786×10^{-6}	1.528×10^{8}
5.88 nm	17	0.281889	4.291×10^{-12}	1.821×10^{-6}	1.890×10^{8}
3.56 nm	10	0.311893	9.160×10^{-12}	1.645×10^{-6}	1.988×10^{8}
2.89 nm	8	0.364484	2.718×10^{-12}	1.408×10^{-6}	2.149×10^{8}
2.29 nm	6	0.36478	1.483×10^{-12}	1.407×10^{-6}	2.150×10^{8}
1.38 nm	4	0.366063	6.812×10^{-15}	1.402×10^{-6}	2.154×10^{8}

2 Results and discussion

Fig. 2b shows a strong agreement between the experimental (solid line) and calculated (signed line) curves of the current in the MIM structure. As the number of h-BN layers increases, the device requires a higher voltage to meet the FN tunneling conditions. Consequently, the device exhibits a significant enhancement in the breakdown voltage, which is the voltage at which the current in the device reaches 1e-11 A.

Fig. 3a depicts the layer-dependent effective mass of h-BN. As the thickness of h-BN increases, the effective mass of electrons in its conduction band decreases. Similar phenomena also exist in other 2D materials[33-34]. When h-BN is in contact with Gold, the variation of the parameters A and B in the FN tunneling effect formula with respect to thickness is shown in Fig. 3b. The parameter A varies inversely with the effective mass, which essentially reflects the influence of effective mass. Meanwhile, the parameter B decreases with the increase of h-BN thickness, in accordance with the behavior of the effective mass. From a physical perspective, it is directly proportional to the effect of the electric field. Under the condition of the same voltage, a thinner h-BN thickness results in a stronger internal electric field, thereby enhancing the likelihood of FN tunneling occurrence. Consequently, the parameter B also becomes larger. Therefore, the accurate determination of the effective mass of the insulator material allows for the precise determination of the parameters of the FN tunneling model.

We further investigated the Gold/h-BN/Gold structure using semiconductor Sentaurus TCAD software, with the h-BN thickness set at 7.54 nm. The FN tunneling model and traps model were both incorporated at the Gold/h-BN interface. We conducted simulations with fixed charge concentrations ranging from 1e11~1e12 cm^{-2} at the Gold/h-BN interface[35] and observed consistent results. Therefore, a single example will be provided for analysis and explanation. According to the simulation results shown in Fig. 4a, regardless of fixed charge densities of 1e11 cm^{-2} or 0, both the F_{ins} and the FN tunneling current density (J_{FN}) remain the same. Since the fixed charge is connected to the power supply through the metal. In an ideal scenario, the power supply is considered a device capable of providing an infinite amount of charge to the device. In contrast, fixed charge defects are very small, and their impact on the device can be neglected. From an alternative perspective, this also serves

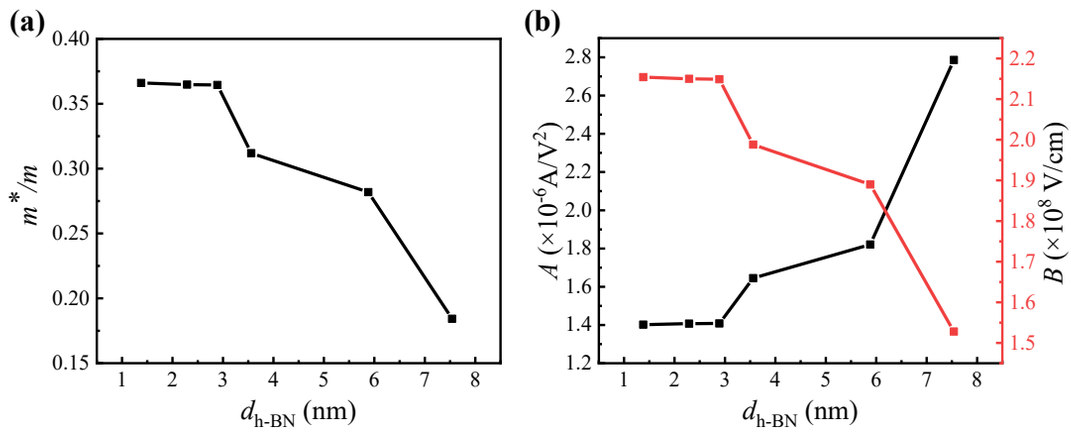

Fig. 3 (a) Effective mass and (b) parameters A, B varies with h-BN thickness
图3 (a) 有效质量及(b) 参数A,B随h-BN厚度变化曲线

as evidence for the validity of the method used to extract the effective mass of h-BN from the *I-V* curve of the MIM structure.

The effect of different metallic materials on FN tunneling effect in h-BN have also been investigated. It is well known that the work function values of nickel (Ni) and tungsten (W) are about 5.2 and 4.6 eV[36-37], respectively. Thus, theoretically we can calculate the φ_B of Ni/h-BN and W/h-BN in contacts to be 3.2 and 2.6 eV, respectively. Then, the parameters A and B of the corresponding FN tunneling model can be obtained precisely. Since the metallic material remains consistent on both sides of the h-BN, the *I-V* characteristics exhibit symmetry under positive and negative bias. As shown in Fig. 4b, the Ni/h-BN/Ni structure has the highest breakdown voltage. Under an applied voltage of 10 V, the J_{FN} in the device is two orders of magnitude smaller than that when W is in contact with h-BN. This difference indicates that the Ni/h-BN contact produces a much higher φ_B than the W/h-BN contact, thereby demanding greater energy for electron traversal across the barrier. However, the higher breakdown voltage of the Ni/h-BN device results in a delayed onset of current flow, leading to lower overall current under the same applied voltage. When extracting the effective mass of h-BN layers using the *I-V* curve of the MIM structure, it is imperative to accurately account for the effect of the metallic material employed. In addition, simulations revealed a direct correlation between the metal work function and device breakdown voltage, with an increase in work function resulting in higher breakdown voltage but lower current. When employing h-BN as a dielectric or tunneling layer, meticulous attention must be paid to the choice of metal materials for contact.

3 CONCLUSIONS

In summary, by employing a research methodology that combines experimental and theoretical approaches, we have successfully studied the effective mass and electrical properties of few-layer 2D h-BN films. The results reveal a distinct correlation that the effective mass consistently decreases with the increasing h-BN film thickness. Furthermore, Sentaurus TCAD simulations have been performed to verify that the fixed charge at the metal/h-BN interface essentially does not influence the FN tunnel-

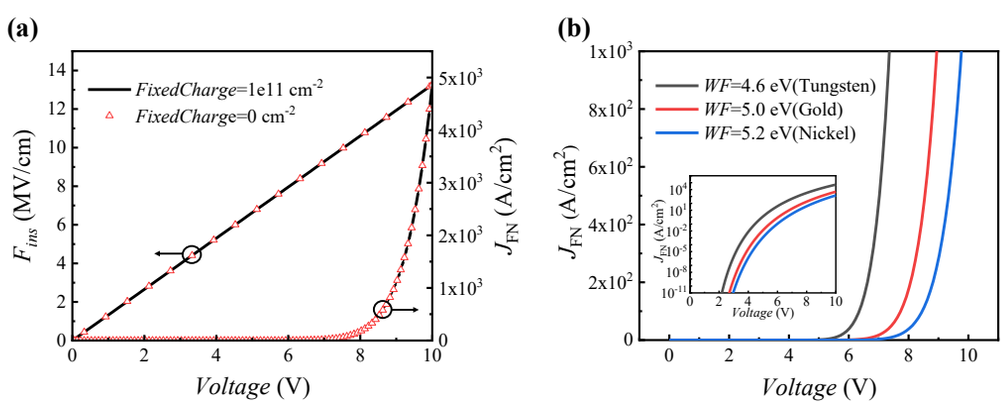

Fig. 4 (a) Effect of fixed charge at the Gold/h-BN interface on FN tunneling. (b) Effect of different metals on FN tunneling when $d_{h\text{-}BN}$ =7.54 nm. The illustration is the J_{FN}-V characteristic curve in logarithmic coordinates.
图4 (a) Gold/h-BN界面处固定电荷对FN隧穿的影响。(b) h-BN厚度为7.54 nm时,不同金属电极对h-BN中FN隧穿的影响。插图为对数坐标下的JFN-V曲线。

ing current, confirming the reliability and accuracy of our approach to extract the h-BN effective mass through the *I-V* curve of the MIM structure. Additionally, different metallic materials significantly affect the FN tunneling in h-BN, which is attributed to the difference in barrier height caused by work function. Overall, this work is of great significance in advancing the application of 2D h-BN atomic layers in fields to be expanded in infrared physics and technology.

References

[1] Lin Y, Connell J W. Advances in 2D boron nitride nanostructures: nanosheets, nanoribbons, nanomeshes, and hybrids with graphene [J]. *Nanoscale*, 2012, **4**(22): 6908-6939.

[2] Shi N, Li L, Gao P, *et al*. Synthesis of Two-Dimensional Hexagonal Boron Nitride and Mid-Infrared Nanophotonics[J]. *ACS Applied Electronic Materials*, 2022, **5**(1): 34-65.

[3] Roy S, Zhang X, Puthirath A B, *et al*. Structure, properties and applications of two-dimensional hexagonal boron nitride [J]. *Advanced Materials*, 2021, **33**(44): 2101589.

[4] Rafiq M, Hu X, Ye Z, *et al*. Recent advances in structural engineering of 2D hexagonal boron nitride electrocatalysts [J]. *Nano Energy*, 2022, **91**: 106661.

[5] Topsakal M, Aktürk E, Ciraci S. First-principles study of two-and one-dimensional honeycomb structures of boron nitride [J]. *Physical Review B*, 2009, **79**(11): 115442.

[6] Chen C, Chen X, Deng B, *et al*. Probing interlayer interaction via chiral phonons in layered honeycomb materials [J]. *Physical Review B*, 2021, **103**(3): 035405.

[7] Cao J, Meng T L, Zhang X, *et al*. On functional boron nitride: electronic structures and thermal properties [J]. *Materials Today Electronics*, 2022: 100005.

[8] Naclerio A E, Kidambi P R. A Review of Scalable Hexagonal Boron Nitride (h-BN) Synthesis for Present and Future Applications [J]. *Advanced Materials*, 2023, **35**(6): 2207374.

[9] Hong S, Lee C S, Lee M H, *et al*. Ultralow-dielectric-constant amorphous boron nitride[J]. *Nature*, 2020, **582**(7813): 511-514.

[10] Pierret A, Mele D, Graef H, *et al*. Dielectric permittivity, conductivity and breakdown field of hexagonal boron nitride [J]. *Materials Research Express*, 2022, **9**(6): 065901.

[11] Bilaç O, Duran C. Al_2O_3/glass/hBN composites with high thermal conductivity and low dielectric constant for low temperature cofired ceramic applications[J]. *Journal of Asian Ceramic Societies*, 2021, **9**(1): 283-290.

[12] Moon S, Kim J, Park J, *et al*. Hexagonal Boron Nitride for Next-Generation Photonics and Electronics [J]. *Advanced Materials*, 2023, **35**(4): 2204161.

[13] Molaei M J, Younas M, Rezakazemi M. A comprehensive review on recent advances in two-dimensional (2D) hexagonal boron nitride [J]. *ACS Applied Electronic Materials*, 2021, **3**(12): 5165-5187.

[14] Kumar A, Low T, Fung K H, *et al*. Tunable light-matter interaction and the role of hyperbolicity in graphene-hBN system[J]. *Nano letters*, 2015, **15**(5): 3172-3180.

[15] Karimkhani H, Vahed H. A broadband optical modulator based on rib-type silicon waveguide including graphene and h-BN layers [J]. *Optik*, 2022, **254**: 168633.

[16] Luo X, Cheng Z, Liu Z, *et al*. Dual-band perfect absorber based on a graphene/hexagonal boron nitride van der Waals hybrid structure [J]. *Journal of Physics D: Applied Physics*, 2021, **54**(37): 375303.

[17] Li J, Maity A, Grenadier S J, *et al*. Charge collection in h-BN neutron detectors at elevated temperatures [J]. *Applied Physics Letters*, 2021, **118**(9).

[18] Xu T, Wang H, Chen X, *et al*. Recent progress on infrared photodetectors based on InAs and InAsSb nanowires [J]. *Nanotechnology*, 2020, **31**(29): 294004.

[19] Hattori Y, Taniguchi T, Watanabe K, *et al*. Determination of carrier polarity in Fowler-Nordheim tunneling and evidence of fermi level pinning at the hexagonal boron nitride/metal interface [J]. *ACS Applied Materials & Interfaces*, 2018, **10**(14): 11732-11738.

[20] Wang J, Ma F, Liang W, *et al*. Electrical properties and applications of graphene, hexagonal boron nitride (h-BN), and graphene/h-BN heterostructures[J]. *Materials Today Physics*, 2017, **2**: 6-34.

[21] Kim Y R, Phan T L, Shin Y S, *et al*. Unveiling the hot carrier distribution in vertical graphene/h-BN/Au van der Waals heterostructures for high-performance photodetector[J]. *ACS Applied Materials & Interfaces*, 2020, **12**(9): 10772-10780.

[22] Lee G H, Yu Y J, Lee C, *et al*. Electron tunneling through atomically flat and ultrathin hexagonal boron nitride [J]. *Applied Physics Letters*, 2011, **99**(24): 243114.

[23] Jang C W, Shin D H, Choi S H. Bifunctional enhancement of photodetection and photovoltaic parameters in graphene/porous-Si heterostructures by employing interfacial hexagonal boron nitride and bathocuproine back-surface passivation layers [J]. *Journal of Materials Chemistry C*, 2022, **10**(42): 15913-15919.

[24] Gao F, Chen H, Feng W, *et al*. High-Performance van der Waals Metal-Insulator-Semiconductor Photodetector Optimized with Valence Band Matching [J]. *Advanced Functional Materials*, 2021, **31**(35): 2104359.

[25] Veeralingam S, Durai L, Yadav P, *et al*. Record-high responsivity and detectivity of a flexible deep-ultraviolet photodetector based on solid state-assisted synthesized hBN nanosheets [J]. *ACS Applied Electronic Materials*, 2021, **3**(3): 1162-1169.

[26] Cheng T T, Zhang K, LUO M, *et al*. Research progress on first-principles calculations of interfacial charge transfer characteristics in InAs-based van der Waals heterojunctions [J]. *Journal of Infrared and Millimeter Waves*, 2023, **42**(5): 666~680.

[27] Jeong H, Bang S, Oh H M, *et al*. Semiconductor-insulator-semiconductor diode consisting of monolayer MoS2, h-BN, and GaN heterostructure[J]. *Acs Nano*, 2015, **9**(10): 10032-10038.

[28] Kim Y R, Phan T L, Shin Y S, *et al*. Unveiling the hot carrier distribution in vertical graphene/h-BN/Au van der Waals heterostructures for high-performance photodetector[J]. *ACS applied materials & interfaces*, 2020, **12**(9): 10772-10780.

[29] Vu Q A, Lee J H, Nguyen V L, *et al*. Tuning carrier tunneling in van der Waals heterostructures for ultrahigh detectivity [J]. *Nano letters*, 2017, **17**(1): 453-459.

[30] Hong S K, Kim J E, Kim S O, *et al*. Flexible resistive switching memory device based on graphene oxide[J]. *IEEE Electron device letters*, 2010, **31**(9): 1005-1007.

[31] Cheon J Y, Kim J H, Kim J H, *et al*. Intrinsic relationship between enhanced oxygen reduction reaction activity and nanoscale work function of doped carbons [J]. *Journal of the American Chemical Society*, 2014, **136**(25): 8875-8878.

[32] Cui Z, He Y, Tian H, *et al*. Study of direct tunneling and dielectric breakdown in molecular beam epitaxial hexagonal boron nitride monolayers using metal-insulator-metal devices [J]. *ACS Applied Electronic Materials*, 2020, **2**(3): 747-755.

[33] Cai Y, Zhang G, Zhang Y W. Layer-dependent band alignment and work function of few-layer phosphorene [J]. *Scientific Reports*, 2014, **4**(1): 6677.

[34] Cai Y, Liu Y, Xie Y, *et al*. Band structure, effective mass, and carrier mobility of few-layer h-AlN under layer and strain engineering [J]. *APL Materials*, 2020, **8**(2).

[35] Jang S K, Youn J, Song Y J, *et al*. Synthesis and characterization of hexagonal boron nitride as a gate dielectric [J]. *Scientific reports*, 2016, **6**(1): 30449.

[36] Zhang T, Wang Y, Zhang Y, *et al*. Comprehensive annealing effects on AlGaN/GaN Schottky barrier diodes with different work-function metals [J]. *IEEE Transactions on Electron Devices*, 2021, **68**(6): 2661-2666.

[37] Raaen S. Adsorption of carbon dioxide on mono-layer thick oxidized samarium films on ni (100)[J]. *Nanomaterials*, 2021, **11**(8): 2064.